CLM - P 478

CLM - P 478

UKAEA

Preprint

THE BUNDLE DIVERTOR-PART II PLASMA PROPERTIES

P E STOTT
C M WILSON
A GIBSON

CULHAM LABORATORY
Abingdon Oxfordshire

1977

CLM-P478

THE BUNDLE DIVERTOR-PART II PLASMA PROPERTIES

P.E. Stott, C.M. Wilson and A. Gibson

Culham Laboratory, Abingdon, Oxon, OX14 3DB, UK
(Euratom/UKAEA Fusion Association)

A B S T R A C T

This paper presents simple estimates of some aspects of the behaviour of plasma in a tokamak with a Bundle Divertor. The effect of the divertor on charged particle orbits, and the consequent changes in cross-field diffusion, are calculated using simple models. The factors determining plasma flow into the divertor are discussed, and a model of the divertor scrape-off layer is used to calculate the exhaust and screening efficiencies. Finally the problems of trapping and pumping the diverted plasma are considered.

(Submitted for publication in Nuclear Fusion)

September 1977
KS

1. INTRODUCTION

The Bundle Divertor [1,2] is a device whose purpose is to improve the purity of a tokamak plasma by reducing the interaction between the plasma and the torus wall. Two divertor coils locally distort the toroidal component of the magnetic field, and divert a bundle of field lines from the outer layer of the plasma into a separate divertor chamber. The magnetic configuration was discussed in detail in an earlier paper [2], and a schematic is shown in figure 1. Whilst it is topologically impossible for the diverted field lines to form perfect magnetic surfaces [3], we have established by numerical computation that the departures of individual field lines from simple surfaces do not seriously impair the effectiveness of the divertor.

An improvement in the plasma purity is expected to result from three specific divertor effects:

(i) Magnetic Limiter The divertor defines a magnetic separatrix, with minor radius a_s, which controls the plasma size without introducing a source of impurities as would a material limiter.

(ii) Plasma Exhaust Charged particles diffusing across the separatrix can flow along the diverted field lines into the divertor chamber, where they are neutralized on a target plate and pumped away. Thus impurities are removed directly along with the exhaust plasma, and the removal of the cold neutral recycling also reduces the influx of impurities from charge-exchange sputtering of the torus wall.

(iii) Screening Layer If the plasma 'scrape-off' layer outside the separatrix is sufficiently thick and dense, any impurity atoms released from the wall, will have a high probability of being ionized in the scrape-off layer and swept into the divertor before they can penetrate deep into the discharge.

In this paper we will discuss the plasma properties of the bundle divertor, and in terms of a simplified model of plasma flow in the scrape-off layer, we will calculate the divertor efficiency. First we consider the orbits of particles following diverted field lines, and in particular those which are reflected by the magnetic mirror region at the entrance of the divertor. In extremely collisionless plasmas, these orbit effects would lead to enhanced cross-field diffusion, and we give some approximate calculations of neoclassical diffusion in section 3. The magnetic mirror also limits the free flow of plasma into the divertor. In section 4 we calculate the exhaust efficiency and in section 5 the screening efficiency of the bundle divertor. Finally we discuss the technological problems of neutralizing and pumping the diverted plasma.

2. PARTICLE ORBITS ON DIVERTED FIELD LINES

The magnetic field strength $|B|$ along a typical diverted field line, is plotted in figure 2a. There are two magnetic mirrors; the familiar toroidal mirror on the inside of the torus, with a relatively weak mirror ratio equal to the inverse aspect ratio $\epsilon = a/R$; and a much stronger mirror with ratio M of the order 2 or 3, on field lines which enter the divertor. An individual field line passes through the toroidal mirror once in every $q = 2\pi/\iota$ transits of the torus, and through the divertor once in every $q_D = 2\pi/\chi_D$ transits, where $\chi_D(r)$ is the acceptance angle of the divertor and ι is the rotational transform. Typically $q \geq 3$ and $q_D \approx 5 - 10$, and the radial dependence is plotted in figure 3.

These two magnetic mirrors divide the velocity space of particles which are following diverted field lines, into three distinct regions as shown in figure 2b.

(1) Diverted particles, $v_\parallel/v_\perp > (M - 1)^{\frac{1}{2}}$, have sufficient parallel velocity to penetrate the strong magnetic mirror at the

entrance to the divertor, and these particles hit the target plate, where they will be neutralized. The fraction of diverted particles in an isotropic velocity distribution is $\gamma_M = 1 - (1 - 1/M)^{\frac{1}{2}} \approx 1/2M$.

(2) Reflected particles, $(M - 1)^{\frac{1}{2}} > v_{\parallel}/v_{\perp} > \epsilon^{\frac{1}{2}}$, are reflected by the divertor mirror, but otherwise pass freely around the torus. In an axisymmetric torus, these would be passing particles, and their drift surfaces are displaced from the corresponding magnetic surface by the order of $\epsilon\rho_\theta$, where ρ_θ is the Larmor radius of the particle in the poloidal field B_θ. This displacement changes sign, when the direction of the particle motion around the torus is reversed, following reflection at the divertor mirror. The projection of a computed particle trajectory onto a radial plane, is shown in figure 4b. This resembles an 'inverted' banana, with turning points at the bundle divertor mirror which is encounted once on every q_D transits of the torus.

(3) Trapped particles, $\epsilon^{\frac{1}{2}} > v_{\parallel}/v_{\perp}$, cannot pass freely around the torus. As in an axisymmetric torus, these trapped particles follow banana orbits, with turning points on the inside of the torus. The banana width is of the order $\epsilon^{\frac{1}{2}}\rho_\theta$, and the trapped fraction of an isotropic distribution $\gamma_T \approx \epsilon^{\frac{1}{2}}$. The bananas themselves drift slowly around the torus, due to a small component of the particle drift velocity parallel to the toroidal field [4]. When a drifting banana encounters the bundle divertor, the trapped particle will be reflected, and the radial drift velocity will change sign. This will lead to a new banana orbit, as shown in figure 4c. After a few such reflections at the bundle divertor, a trapped orbit will intersect the torus wall.

These general predictions have been confirmed [5] by computing the guiding centre orbits of particles with different values of $v_{\parallel}/v_{\perp}$, using a program developed from that described by Gibson and Taylor [6].

Typical projections onto a radial plane are shown in figure 4.

Single-particle orbits which pass close to the stagnation point have been computed and projections of typical orbits onto the horizontal plane are shown in figure 5 together with contours of the magnetic field strength $|B|$. These well-behaved examples of diverted and undiverted orbits were started in an unperturbed plane of the torus at points displaced by an ion Larmor radius (in the unperturbed toroidal field) from the separatrix field line. Orbits started closer to the separatrix are less well-behaved and experience larger displacements in the low-field region which may intercept the central support of the divertor coil. These computations confirm our earlier predictions [2] that the width of the loss-region surrounding the separatrix is of the order of an ion Larmor radius measured on the unperturbed toroidal field. For typical tokamak parameters this loss would not exceed 10% of the diverted plasma flux.

Trapped particle effects play a major role in the neoclassical theory of plasma diffusion and heat conduction, for rarefied plasmas in axisymmetric tori. In the following section we will consider the enhancement of these transport processes by the additional particle trapping due to the bundle divertor.

3. ESTIMATES OF BINARY COLLISIONAL TRANSPORT

In an axisymmetric torus, neoclassical transport theory is conveniently divided into three regimes of collision frequency; $\nu < \nu_1$, collisionless or banana regime; $\nu_1 < \nu < \nu_2$, intermediate or plateau regime; $\nu_2 < \nu$, collisional or Pfirsch-Schluter regime. Two characteristic frequencies separate these three regimes; $\nu_2 = v_{th}/qR$ is the transit frequency around the torus of passing particles with $v_{\parallel} = v_{th}$, where $v_{th} = (2kT/m)^{\frac{1}{2}}$ is the thermal velocity; $\nu_1 = \epsilon^{\frac{3}{2}}\nu_2$ is the bounce frequency

of trapped particles on a banana orbit.

The familiar form of the dependence of the neoclassical transport coefficients on collision frequency ν is shown in figure 6a. Approximate expressions for the ambipolar diffusion coefficient in each regime are: $D_\perp$ (Pfirsch-Schluter) $\approx \rho_e^2 \nu_{ei} (1 + q^2)$; $D_\perp$ (plateau) $\approx \rho_e^2 \nu_2 (1 + q^2)$; $D_\perp$ (banana) $\approx \epsilon^{-\frac{3}{2}} \rho_e^2 \nu_{ei} (1 + q^2)$, where $\rho_e = (2kTm)^{\frac{1}{2}} e/c B_\varphi$ is the electron Larmor radius in the toroidal field B_φ, and ν_{ei} is the electron-ion collision frequency.

The bundle divertor modifies the banana orbits of the toroidally-trapped particles and reflects the bulk of the passing particles on the outer flux surfaces into inverse banana orbits. Only the relatively small group of particles with $v_\parallel/v_\perp > (M - 1)^{\frac{1}{2}}$, which we have called the 'diverted particles' can penetrate the strong divertor mirrors. These new orbits modify the neoclassical transport coefficients in the divertor scrape-off layer, although, as we will see below, the changes are important only for extremely low collision frequencies which are unlikely to be encountered in the plasma boundary region.

The simplest case is that of a dense plasma, $\nu > \nu_2$. All of the particles suffer many collisions in the course of a single transit around the torus, and the trapped and reflected particles cannot complete their characteristic orbits. The influence of the bundle divertor mirrors can be neglected and the collisional Pfirsch-Schluter transport coefficients still apply.

As the collision frequency ν is reduced below ν_2, particles with large values of $v_\parallel$ can make collision-free transits of the torus. The parallel transit time to the divertor for a particle with $v_\parallel \approx v_{th}$ is $t_\parallel \approx q_D R/v_{th}$. It is convenient to define a characteristic divertor frequency, $\nu_3 = t_\parallel^{-1} = v_{th}/q_D R = \nu_2 q/q_D$. The diverted particles occupy a narrow cone in velocity space, with $v_\perp \approx v_{th}/M^{\frac{1}{2}}$, and the effective

collision frequency for scattering out of this cone is $\nu_{eff} = \nu(v_{th}/v_\perp)^2 \approx \nu M$, where ν is the collision frequency for 90^o scattering. The diverted particles make collisionless flight to the divertor if $\nu_{eff} < \nu_3$, ie $\nu < \nu_3/M$.

The reflected particles, $(M-1)^{\frac{1}{2}} > v_\parallel/v_\perp > \epsilon^{\frac{1}{2}}$, comprise the largest group in the distribution. The time taken to complete an inverse banana orbit is of the order $t_i \approx q_D R/v_\parallel$, and as the collision frequency is reduced below ν_3, the first complete inverse bananas are those for particles with the largest values of parallel velocity, ie $v_\parallel \approx v_{th} (M-1)^{\frac{1}{2}}/M^{\frac{1}{2}}$. The width of an inverse banana orbit is of the order $\Delta x \approx V_\perp t_t$, where $V_\perp \approx \rho v_{th}/R$ is the transverse drift velocity across the toroidal field and $t_t \approx qRM^{\frac{1}{2}}/v_{th} (M-1)^{\frac{1}{2}}$ is the time for a reflected particle to make a single transit of the minor circumference. Thus the width of the first, and thinnest, inverse banana is $\Delta x \approx \rho q (M/(M-1))^{\frac{1}{2}}$. As ν is further reduced, reflected particles with smaller and smaller values of $v_\parallel$ will have sufficient time between collisions to complete their orbits. The last inverse banana appears when $\nu = \epsilon^{\frac{1}{2}} \nu_3$ for particles with $v_\parallel/v_\perp \approx \epsilon^{\frac{1}{2}}$ which are almost slow enough to be trapped by the toroidal field. This is also the 'fattest' inverse banana, $\Delta x \approx \rho q \epsilon^{-\frac{1}{2}}$. These reflected particles must be scattered through large angles before they escape through the divertor mirrors, and thus the effective collision frequency is of the order of ν, the 90 degree collision frequency. The diffusion coefficient corresponding to the inverse bananas is obtained by averaging the inverse banana width over all the reflected particles in the range $(M-1)^{\frac{1}{2}} > v_\parallel/v_\perp > \epsilon^{\frac{1}{2}}$. Thus $D_\perp \approx \langle \Delta x^2 \rangle \nu \approx \rho^2 q^2 \nu \epsilon^{-\frac{1}{2}}$. The complete dependence on collision frequency is similar to that for trapped particles in an axisymmetric torus and is plotted in figure 6b.

When the collision frequency is reduced below ν_1, the toroidally-trapped particles, $v_\parallel/v_\perp < \epsilon^{\frac{1}{2}}$, have sufficient time between collisions to complete banana orbits. The transit time of the orbit is approximately $t_b \approx q\,R/v_\parallel \approx (\nu_2\,\epsilon^{\frac{1}{2}})^{-1}$. The typical banana width is $\Delta x \approx V_\perp t_b \approx \rho q\,\epsilon^{-\frac{1}{2}}$. Particles remain trapped following small-angle collisions only if $\Delta v < v_{th}\,\epsilon^{\frac{1}{2}}$, and thus the effective collision frequency is of the order $\nu_{eff} \approx \nu(v_{th}/\Delta v)^2 \approx \nu/\epsilon$. Banana diffusion of the trapped particles, a fraction of the order of $\epsilon^{\frac{1}{2}}$ of the total number of particles, dominates the transport coefficients in the collisionless regime. This leads to a simple estimate of the well-known banana diffusion coefficient, $D_\perp \approx \epsilon^{\frac{1}{2}}\,(\Delta x)^2\,\nu_{eff} \approx \epsilon^{-\frac{3}{2}}\,\rho^2 q^2\,\nu$.

When a trapped particle drifts into the bundle divertor mirror it is reflected onto a new banana orbit, and successive reflections between the toroidal and divertor mirrors lead to the class of particle orbits shown in figure 4c which eventually escape from the containment system. The fraction of banana orbits which intersect the divertor at any one time is equal to q/q_D, and thus the bounce frequency of bananas with the divertor is $\nu_2\,\epsilon^{\frac{1}{2}}\,q/q_D = \nu_3\,\epsilon^{\frac{1}{2}}$. These loss orbit effects cause enhanced diffusion at very low collision frequencies $\nu < \gamma_3\,\epsilon^{\frac{1}{2}}$ as shown in figure 6c, similar to that produced by super banana diffusion in stellarators.

4. PLASMA FLOW INTO THE DIVERTOR

We will now consider the flow of plasma into the bundle divertor, and calculate the thickness of the scrape-off layer surrounding the main body of the discharge and the exhaust efficiency. We have already seen that the flow of plasma into the bundle divertor is impeded, because individual field lines do not pass through the divertor on each transit of the torus, and also because a large fraction of the particles following these

field lines is reflected by the strong magnetic mirrors at the divertor entrance. Particles which are initially unable to penetrate the divertor mirror must be contained within the scrape-off layer long enough for collisions to scatter them into the mirror loss-cone. The density profile in the scrape-off layer is determined by this balance between restricted flow along field lines into the divertor, and radial transport across the field lines. The parameters of the scrape-off layer plasma depend on the parameters of the contained plasma inside the separatrix, which in turn depend on the efficiency of the divertor in controlling recycling and impurity influx.

We will not attempt to solve this problem self consistently but will consider a simple, one-dimensional model of the scrape-off layer, as shown schematically in figure 7, characterised by a radial diffusion coefficient $D_{\perp s}$, and a particle loss time to the divertor $t_{\parallel}$. In a sufficiently dense plasma, particles will be scattered by collisions into the loss-cone of velocity space in a shorter time than their transit time along field lines into the divertor. The isotropic velocity distribution will be maintained when $\nu > \nu_z/M$, and for typical divertor parameters, $q_D \sim 5$, $R \sim 120$ cm, $M \sim 3$, this condition is satisfied when the scrape-off layer density (in cm^{-3}) $n_s > 7 \times 10^7 T^2$, where T is the plasma temperature in eV. The loss rate to the divertor is then determined by the parallel flow velocity along diverted field lines. In order to maintain an ambipolar flow into the divertor, a sheath will form in front of the target plate, setting up an electrostatic field which will repel electrons and accelerate ions into the target. We will assume that the divertor target is electrically isolated from the torus, so that the radial

and parallel plasma fluxes are independently ambipolar. The ambipolar flux into the divertor will have a velocity of the order of the ion sound speed, $v_s \approx (2kT_e/m_i)^{\frac{1}{2}}$. The particle flux into the divertor will be of the order $(2\pi/q_D) a_s n_d v_s dx$ where $n_d \approx n/2M$ is the fraction of particles in the divertor loss-cone. The continuity equation for particles in the scrape-off layer is

$$D_{\perp s} \frac{d^2 n}{dx^2} = \frac{v_s}{4\pi R M q_D} n,$$

where $x = r - a_s$ is the distance into the scrape-off layer from the separatrix $r = a_s$.

Neglecting the parametric dependence of $D_\perp$ and v_s, and taking an average value for q_D across the scrape-off layer, gives a solution of the form

$$n(x) \approx n_s \exp(-x/\Delta)$$

where $\Delta = (D_{\perp s} 4\pi R M q_D / v_s)^{\frac{1}{2}} \approx (D_{\perp s} M/\nu_3)^{\frac{1}{2}}$ and n_s is the density at the separatrix. More detailed models of the divertor scrape-off layer [7,8,9] give different functional forms for the density profile, but the scale length $\Delta = (d\ell n\, n/dx)^{-1}$ does not differ significantly from that given by the simplified model.

In order to evaluate the expression for the density scale-length in the scrape-off layer, we have assumed that the cross-field diffusion coefficient follows the Pfirsch-Schluter dependence but with $D_{\perp s} \approx 100\, D_{ps}$, where the enhancement factor was determined empirically on DITE [10]. Calculated values of Δ for densities and temperatures typical of the scrape-off layer are plotted in figure 8. Recent measurements [16] on DITE with $B_\varphi = 10$ kG, $n_s = 4 \times 10^{12}$ cm^{-3} and $T_e = 30$ eV give $\Delta \approx 4.8$ cm which is in good agreement with the calculated value of $\Delta = 3.8$ cm.

We can define the exhaust efficiency of the bundle divertor as $\xi_x = 1 - \exp(-(a_L - a_s)/\Delta)$ where a_L is the minor radius of the torus wall or protective limiter. Values of ξ_x are plotted on the right hand side of figure 8 for $a_L - a_s = 0.25\ a_s$ which corresponds approximately to the DITE values $a_L = 27$ cm, $a_s = 21$ cm.

In a less dense or hotter plasma, $\nu < \nu_z/M$, the diverted particles would be collisionless, and would be captured by the divertor faster than collisions can scatter reflected and trapped particles into the loss cone. The particle flux to the divertor would be determined by the rate at which collisions can fill the loss-cone. The continuity equation becomes

$$D_{\perp s} \frac{d^2 n}{dx^2} = \nu n$$

with a solution of the form $n(x) = n_s \exp(-x/\Delta)$ where $\Delta = [D_{\perp s}/\nu]^{\frac{1}{2}}$ and ν is the 90° collision frequency for the ions. The anisotropic velocity distribution caused by the divertor loss-cone may be unstable to several velocity-space modes. These instabilities, if they develop, are unlikely to be damaging to the confinement but may scatter particles into the loss-cone, thus usefully enhancing ν.

5. SCREENING EFFICIENCY

The bundle divertor inherently produces a much thicker scrape-off layer than is the case for a poloidal field divertor and should provide good impurity screening. The screening process comprises two stages; first there is the probability that an incoming, low-energy impurity atom will be ionized in the scrape-off layer, and then there is the probability that the ion will be swept into the divertor before it diffuses inside the separatrix. In calculating the screening efficiency we will consider a simplified model and assume that the

inward diffusion is sufficiently slow that all the ions are swept into the divertor. With this simplification we set the screening efficiency equal to the ionization probability.

$$\xi_s = 1 - \exp\left(1 - \int_{a_L}^{a_s} n \frac{\langle \sigma v_e \rangle}{v_I}\right) = 1 - \exp\left(- \xi_x \Delta n_s \frac{\langle \sigma v_e \rangle}{v_I}\right),$$

where $\langle \sigma v_e \rangle$ is the ionization rate [11,12], and v_I is the velocity of the incident neutral impurity, which we assume to have an energy of 1 eV. In figure 9 we have plotted the screening efficiencies for typical light impurities (oxygen) and heavy impurities (iron). The calculated values of ξ_s are close to unity for iron when $n_s > 2 \times 10^{12}$ cm^{-3} and for oxygen when $n_s > 1.0 \times 10^{13}$ cm^{-3}. Experimental results from DITE [10, 13] indicate good screening of carbon, oxygen, molydbenum and iron but the screening efficiency has so far not been measured quantitatively.

6. TRAPPING AND PUMPING THE DIVERTED PLASMA

The diverted plasma is directed onto a target which has two main functions.

(i) To neutralise and trap the ions.

(ii) To absorb the plasma energy.

The divertor target should be a material with a high trapping probability for incident hydrogen ions. Metals such as titanium, zirconium, niobium etc have trapping probabilities as high as 90% for hydrogen ions with energies of several keV [14]. Trapping efficiences are lower at lower energies, but recent measurements indicate that efficiences of 50% may be attained for 300 eV protons on zirconium surfaces which are free from oxide contamination [15]. This surface conditioning can be achieved by baking the target in a clean, ultra-high vacuum environment. Alternatively a freshly-deposited getter layer of titanium may be useful for trapping low-energy ions.

Those ions which are not trapped are assumed to be back scattered inelastically after depositing most of their energy in the target. In DITE, this gas is pumped away on active titanium gettered surfaces deposited on the walls of the target chamber and in a separate divertor pumping tank. The total pumping speed of the DITE system, is ~ 5×10^4 ℓsec^{-1} at the target, and we calculate that about 15% of the untrapped particles will return to the torus. The efficiency of the divertor is impaired by this return of gas to the torus and it is important to maximise the trapping efficiency of the target so as to minimise the gas load on the pumping system.

The trapping efficiency of metal surfaces falls off sharply at low temperatures (eg 200 K for titanium), and at high temperatures (600 K for titanium). It is important to maintain the surface temperature of the target within these limits. We have designed a target which can be outgassed by baking, and then pre-cooled to ~ 200 K so as to utilise the optimum temperature range for trapping. It is particularly important that the surface temperature does not rise above 600 K during the discharge, since this would cause previously absorbed gas to be desorbed rapidly giving a large pressure rise in the torus. This may necessitate moving the target during the plasma pulse to increase the effective exposed surface area. The trapping efficiency of typical target materials also falls sharply after the surface has absorbed a large dose, and after each experimental shot the target should be baked in order to desorb the particles previously trapped and to ensure a clean, activated surface for the next pulse.

7. CONCLUSIONS

We have discussed the plasma properties of the bundle divertor, and have made calculations of these effects using simplified models.

The magnetic mirror region at the entrance of the divertor introduces new types of particle orbits which lead to enhanced cross-field diffusion rates in very collisionless plasmas. These effects will be unimportant in parameter regimes applicable to present-day experiments, but may be important considerations in considering possible extrapolations to more collisionless reactor regimes.

We have calculated the flow of plasma into the divertor and obtained estimates for the density gradient in the scrape-off layer which are in good agreement with preliminary experimental results from DITE. Using these estimated values for the density gradient, we have calculated the screening efficiencies for heavy and light impurities, and have shown that these can be close to unity. The good screening action of the DITE bundle divertor has been demonstrated experimentally. Finally we have considered the technological problems of trapping and pumping the diverted plasma.

REFERENCES

[1] COLVEN, C., GIBSON, A., and STOTT, P.E., Proceedings of the 5th European Conf. on Controlled Fusion and Plasma Physics, Grenoble (1972).

[2] STOTT, P.E., WILSON, C.M., and GIBSON, A., Nuclear Fusion 17 481 (1977).

[3] TAYLOR, J.B., Culham Laboratory Report CLM R132 (1974).

[4] KADOMTSEV, B.B., and POGUTSE, O.P., Nuclear Fusion 11, 67 (1971).

[5] STOTT, P.E., COLVEN, C., and GIBSON, A., A.P.S. Plasma Physics Division Meeting, Philadelphia (1973).

[6] GIBSON, A., and TAYLOR, J.B., Phys. Fluids 10, 2653 (1967).

[7] HASSELBERG, G., and ROGISTER, A., Private communication.

[8] MENSE, A.T., and EMERT, G.A., Bull. Am. Phys. Soc. 18, 1305 (1973).

[9] BOOZER, A.H., Princeton University Report MATT 1149.

[10] PAUL, J.W.M., et al, 6th IAEA Conf. on Plasma Physics and Controlled Nuclear Fusion Research, Berchtesgaden, Paper IAEA-CN-35/A17 (1976) and HUGILL, J., Private communication.

[11] LOTZ, W., Institut fur Plasmaphysik, Garching bei Munchen, Report IPP 1/62 (1967).

[12] MATTIOLI, M., Fontenay-aux-Roses Report EUR-CEA-FU 761 (1975).

[13] STOTT, P.E., et al Symposium on Plasma-Wall Interactions, Julich (1976).

[14] McCRACKEN, G.M., JEFFERIES, D.K., and GOLDSMITH, P., Proc. 4th International Vac. Conf. Inst of Physics 149 (1968).

[15] BOHDANSKY, J., ROTH, J., POSCHENRIEDER, Proc. of Conf. on Applications of Ion Beams to Materials, Inst. of Physics 307 (1976).

[16] STOTT, P.E., et al, The Bundle Divertor - Part III Experimental Results - to be published.

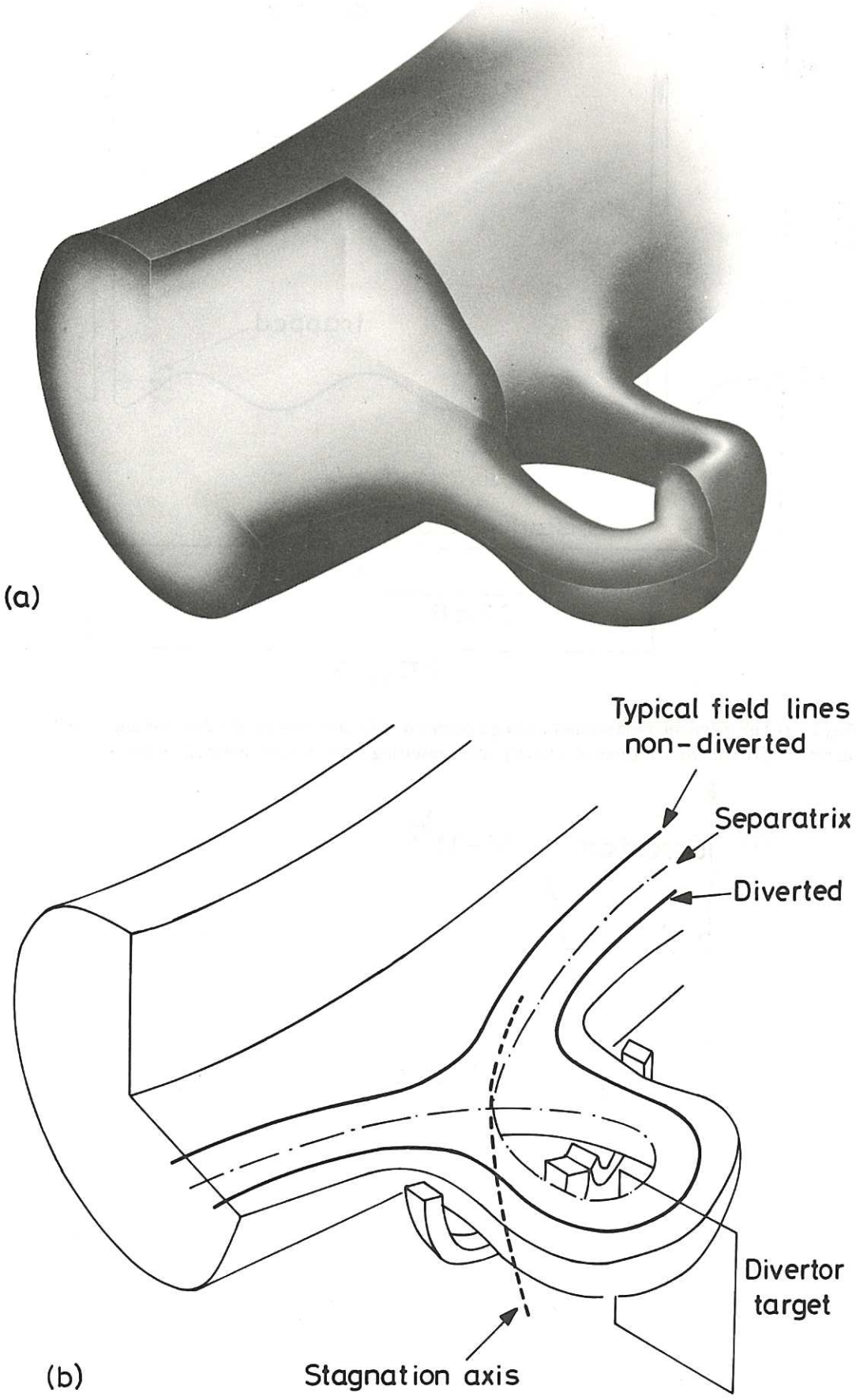

Fig.1 Schematic of the bundle divertor, and a cut-away section showing the principal features of the magnetic configuration.

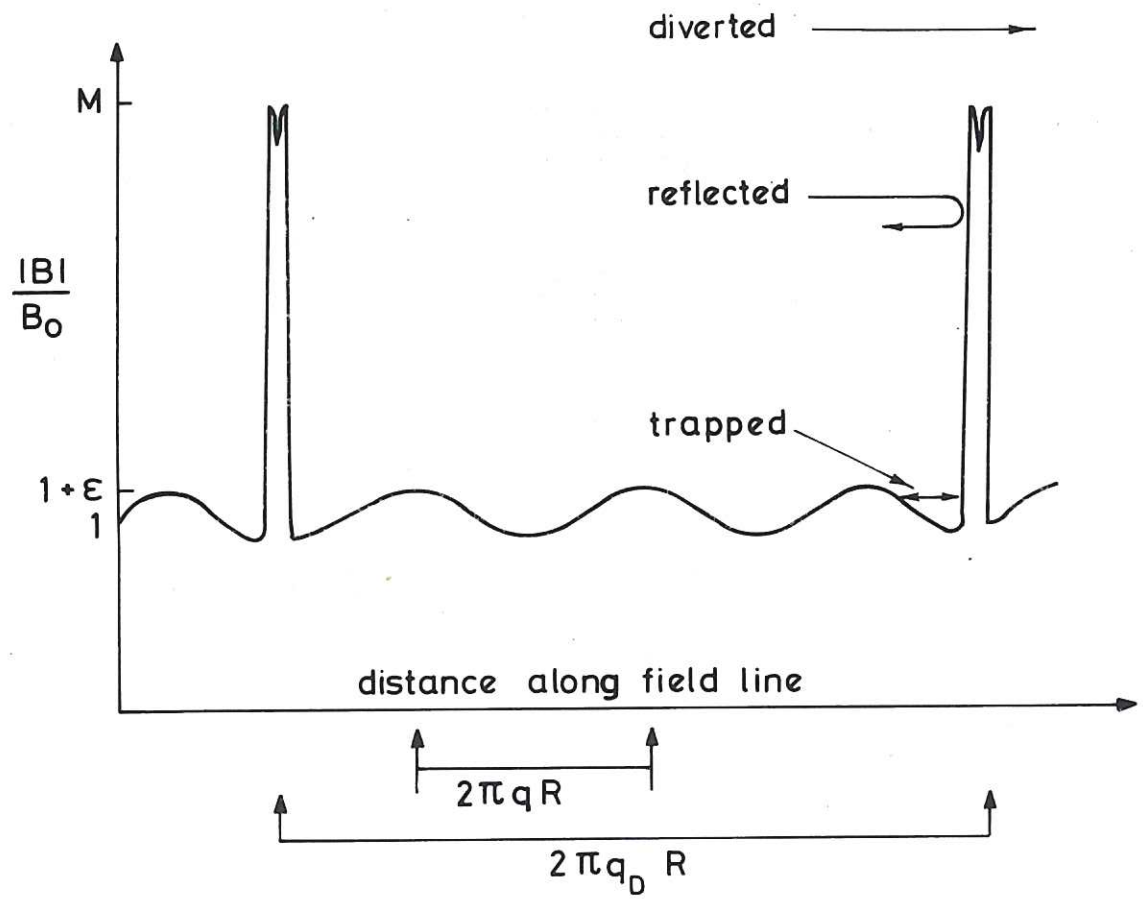

Fig.2 (a) The magnetic field strength along a diverted field line showing the divertor and toroidal magnetic mirrors. (b) The three regions of velocity space resulting from the two magnetic mirrors.

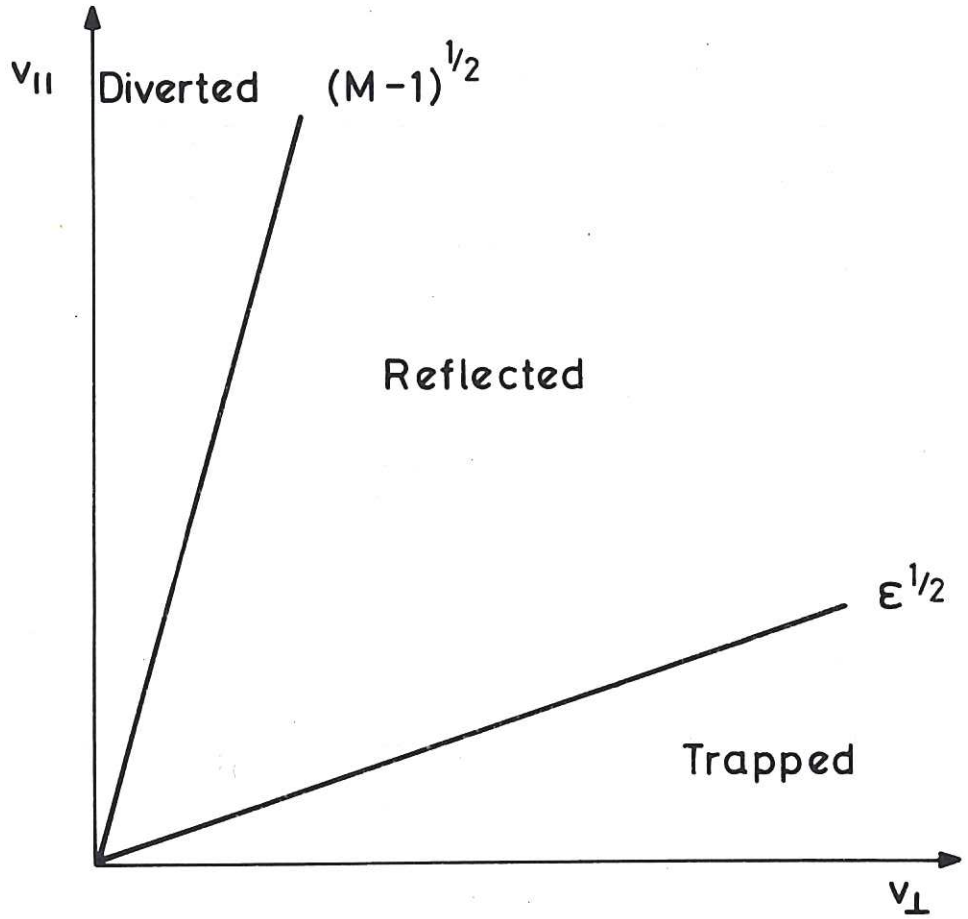

Fig.2 (b) The three regions of velocity space resulting from the two magnetic mirrors.

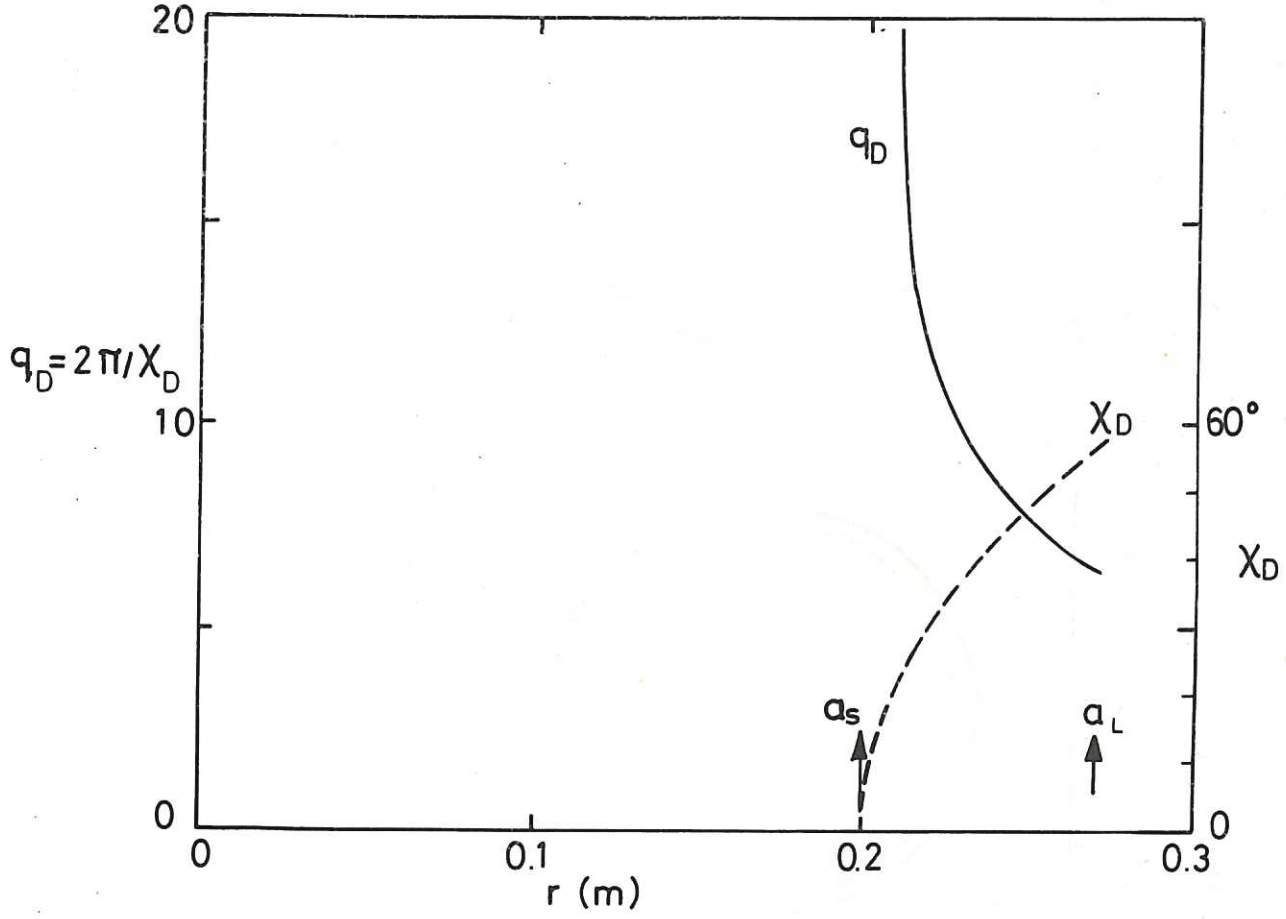

Fig.3 Divertor acceptance angle χ_D and the frequency with which field lines are diverted $q_D = 2\pi/\chi_D$ as a function of radius.

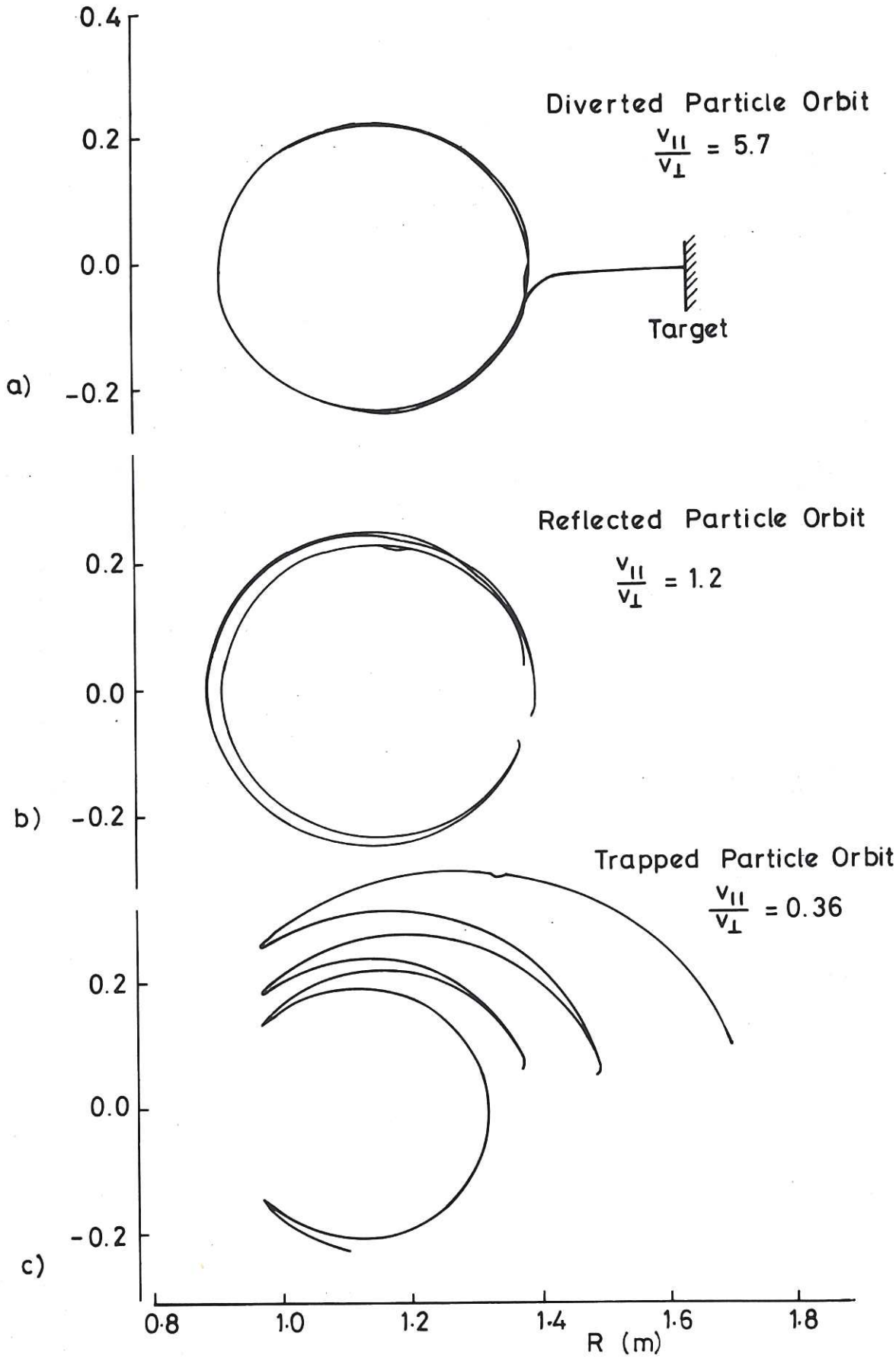

Fig.4 Projections onto a radial plane of guiding-centre orbits for typical diverted, reflected and trapped particles.

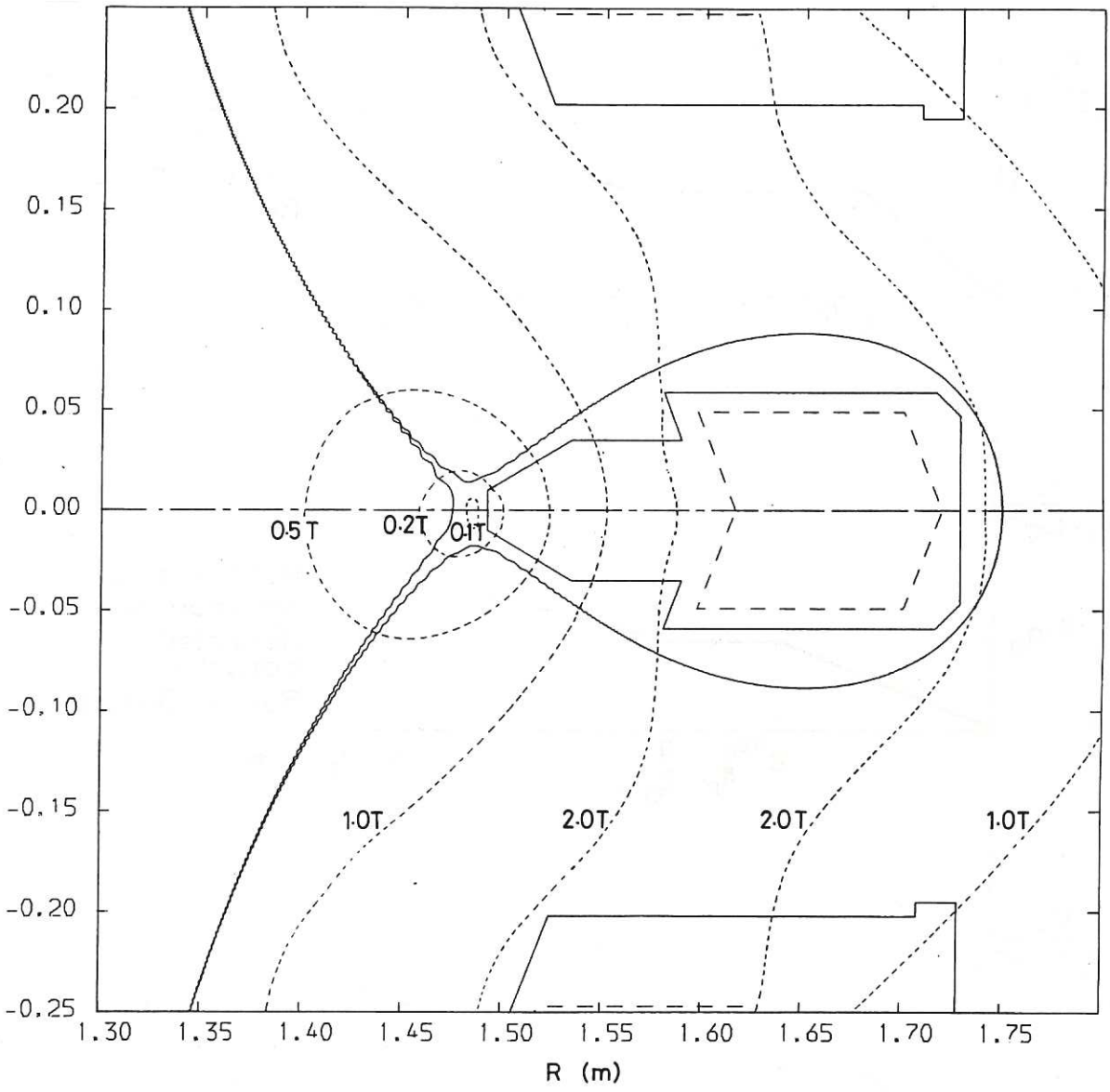

Fig.5 Projections onto the horizontal plane of typical single-particle orbits which pass close to the stagnation region. The dotted lines show contours of the magnetic field strength |B| normalised to B_ϕ = 1.0T at R = 1.17m.

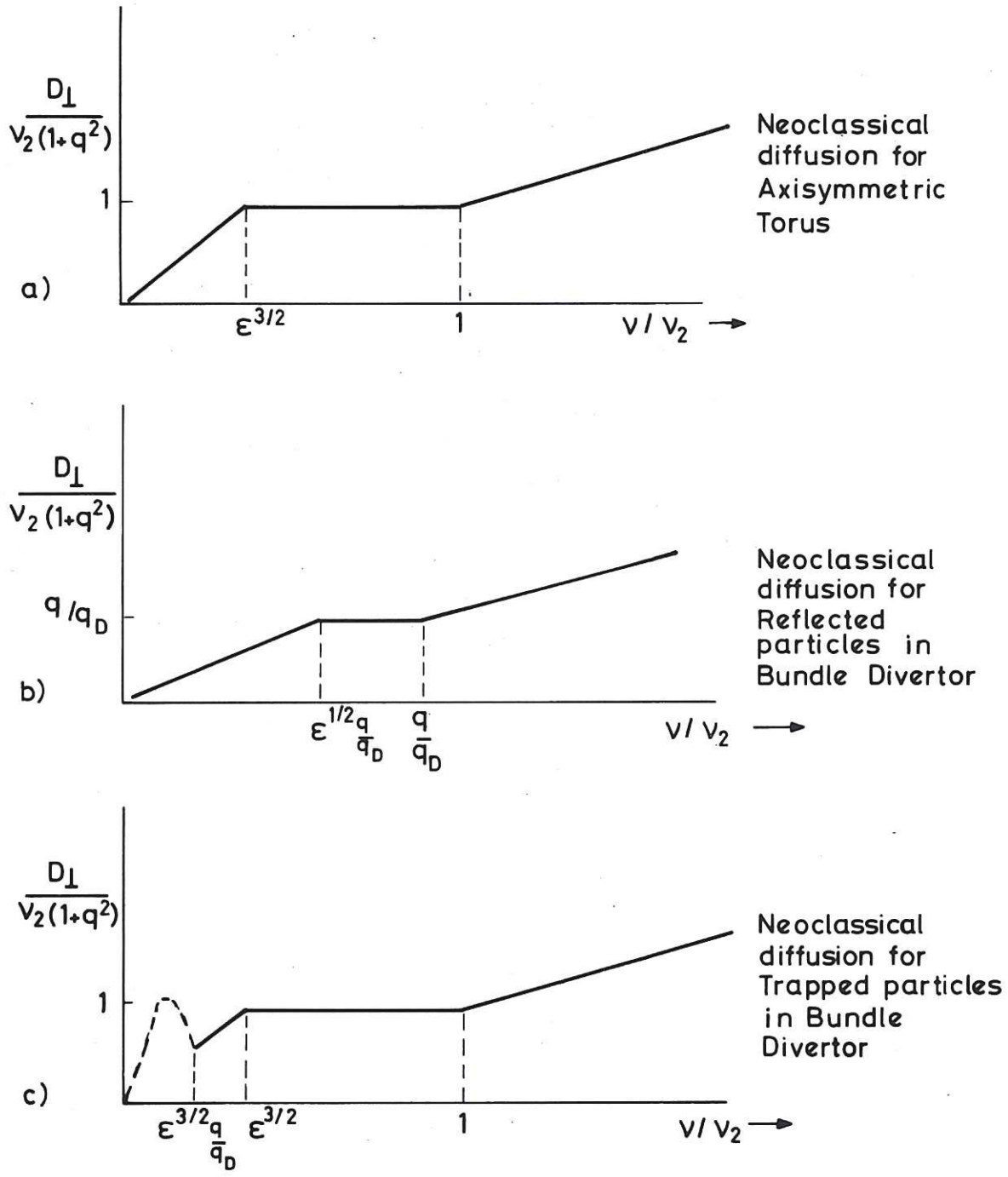

Fig.6 Approximate dependence of particle diffusion coefficient $D_\perp$, on collision frequency γ.

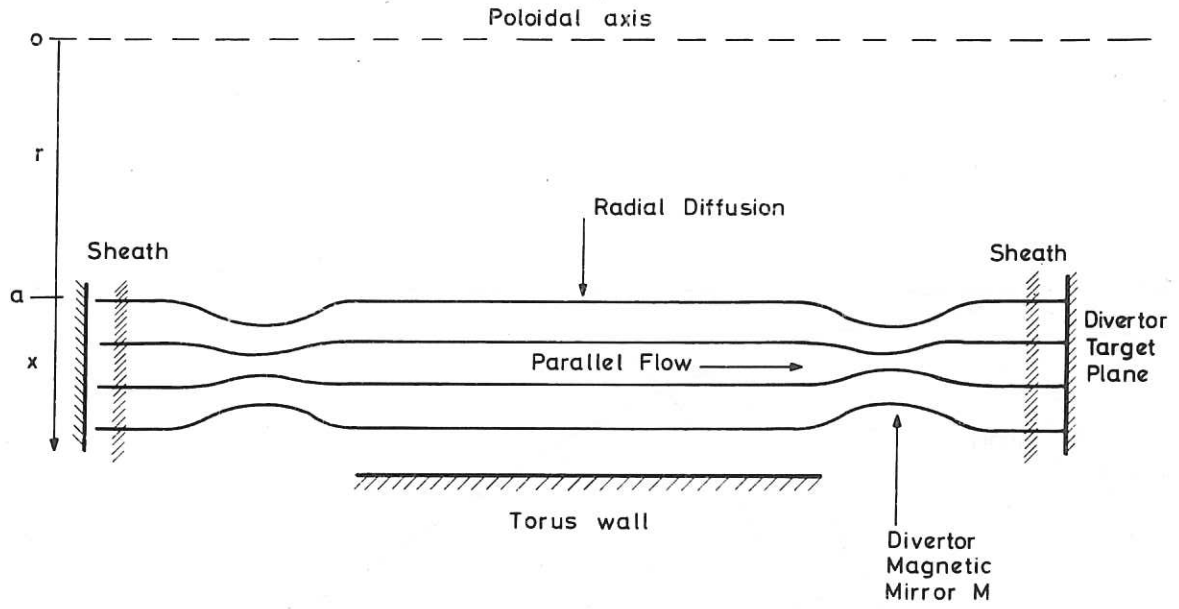

Fig.7 A one-dimensional model of the divertor scrape-off layer.

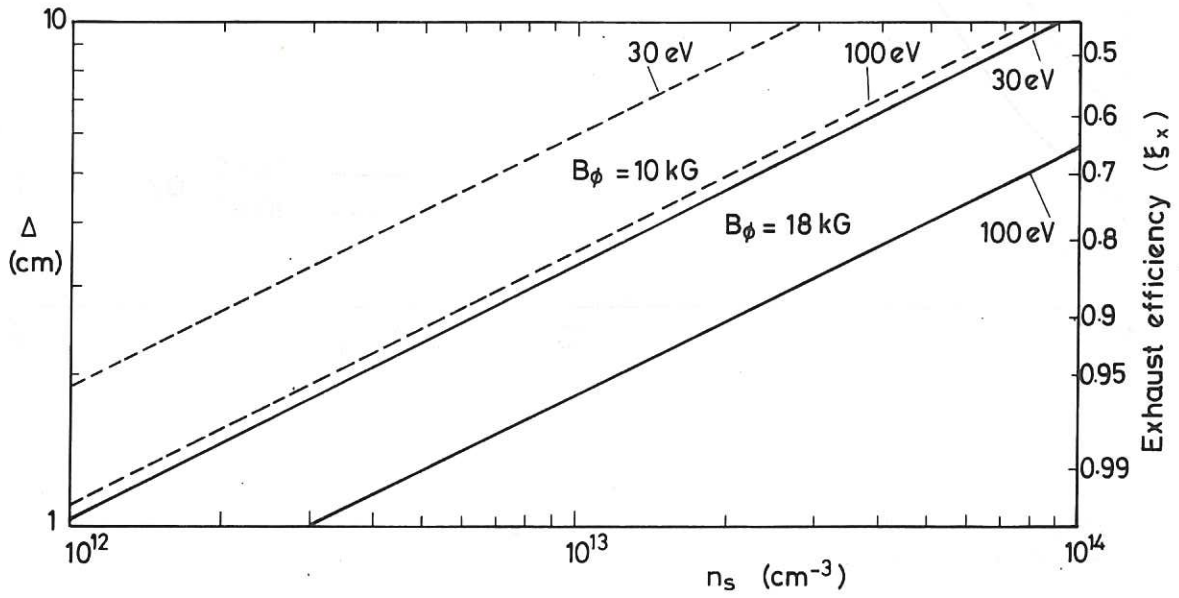

Fig.8 Density scale length $\Delta = [d\ \ell n\ n/dx]^{-1}$ in the scrape-off layer for typical densities and temperatures.

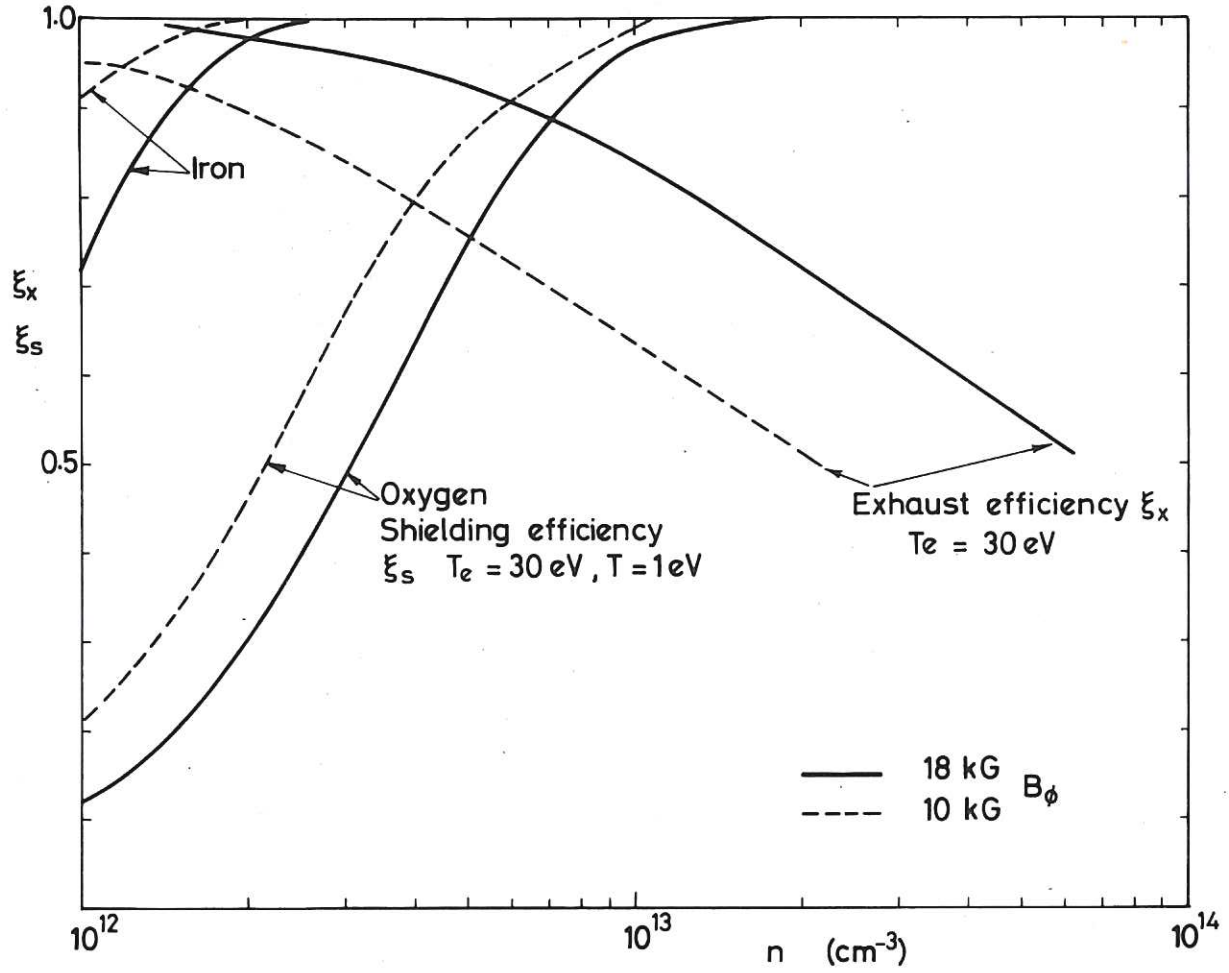

Fig.9 Exhaust (ξ_x) and screening (ξ_s) efficiencies for oxygen and iron impurities as a function of the scrape-off layer density.